Oriented silver chloride microcrystals and nanocrystals embedded in a crystalline KCl matrix, as studied by means of electron paramagnetic resonance and optically detected magnetic resonance

2001 J. Phys.: Condens. Matter 13 2651

(http://iopscience.iop.org/0953-8984/13/11/320)

INSTITUTE OF PHYSICS PUBLISHING JOURNAL OF PHYSICS: CONDENSED MATTER

J. Phys.: Condens. Matter **13** (2001) 2651–2669 www.iop.org/Journals/cm PII: S0953-8984(01)20503-7

Oriented silver chloride microcrystals and nanocrystals embedded in a crystalline KCl matrix, as studied by means of electron paramagnetic resonance and optically detected magnetic resonance

P G Baranov, N G Romanov, V A Khramtsov and V S Vikhnin

Ioffe Physico-Technical Institute, Russian Academy of Sciences, 26 Politekhnicheskaya Street, 194021 St Petersburg, Russia

E-mail: nikolai.romanov@pop.ioffe.rssi.ru

Received 5 January 2001

Abstract

Self-trapped holes (STH), self-trapped excitons (STE) and shallow electron centres in small AgCl crystals embedded in a KCl crystalline matrix have been observed by means of optically detected magnetic resonance (ODMR). The existence of the impurity clusters in heavily doped KCl:AgCl single crystals, ranging from single and paired Ag ions to AgCl nanometre- and micrometre-size crystals (nanocrystals and microcrystals) retaining the orientation of the matrix, was confirmed. ODMR spectra were used as a fingerprint of the embedded AgCl microcrystals and a signature of their crystallinity. For AgCl nanocrystals the anisotropy of the g-factor both for isolated STH and for STH forming STE was found to be substantially reduced compared with those of bulk AgCl crystals and AgCl microcrystals embedded in KCl. This implies a considerable suppression of the Jahn–Teller effect in nanoparticles. A rather general mechanism of the suppression of the Jahn–Teller effect in nanocrystals is developed, taking into account the additional deformation field appearing because of the strong vibronic interaction at the interface. It allows evaluation of the critical size of the embedded AgCl nanocrystals, at which the suppression of the Jahn–Teller effect has its onset; the value obtained is $\approx$10 nm, in agreement with experiment.

1. Introduction

Nowadays semiconductor and solid-state physics appears to be the physics of systems with reduced dimensionality. Fabrication of single or periodic potential wells by simply combining two materials with different energy gaps and spatial dimensions confining the motion of electrons and holes results in exciting new effects that originate in the size dependence of quantum phenomena.

0953-8984/01/112651+19$30.00

In the last decade, nanostructures have been successfully fabricated using self-organization effects common to strained heterosystems [1]. Fabrication of new structures and devices based on anisotropic nanoparticles is of great interest since anisotropic particles can exhibit novel and enhanced properties compared with those of isotropic spherical particles. Semiconductor nanocrystals have been mainly studied for II–VI semiconductors dispersed in vitreous matrices [2, 3]. However, nanocrystals can show a common orientation only in a crystalline matrix, as recently demonstrated for CuCl and AgCl nanocrystals embedded in an alkali halide matrix [4–8].

It is well known that the electronic, as well as atomic, structure is considerably changed as the size increases from clusters to small particles and, finally, to a bulk material, as a result of which manifold interesting properties are developed. In this respect, KCl:AgCl seems to be a very promising system in which to study these effects. It has long been known that silver ions Ag^+ substitute for alkali ions in silver-doped alkali halide crystals. Ultra-violet (UV) light or x-ray irradiation can produce a number of different silver-related point defects [9–11]. On the other hand, silver halide nanometre- and micrometre-size crystals, i.e. nanocrystals and microcrystals, can be formed in the growth of KCl single crystals heavily doped with AgCl, as recently reported in [6–8]. KCl and AgCl have the same face-centred cubic lattice with the lattice constants $2a = 0.629$ nm and $2a = 0.555$ nm, respectively. The energy gaps are 8.7 eV for KCl and 3.26 eV for AgCl. Thus, AgCl crystals embedded in KCl can be considered as an array of self-organized microcrystals and nanocrystals (quantum dots) in a strained KCl:AgCl heterosystem.

Silver halides exhibit some unique features and occupy an exceptional position in solid-state physics since their properties can be regarded as lying at the borderline between ionic and covalent bonding [12]. They play an important role in the photographic industry, being among the few materials in which latent images are formed. In order to get a better understanding of this process, it is important to learn more about the intrinsic properties of the material, particularly when one goes from bulk materials to the micrometre and nanometre scale where the materials are known to behave quite differently because of the quantum effects.

Under UV light irradiation of AgCl, an electron is excited from the valence band into the conduction band and a hole is left in the valence band, where it can undergo self-trapping to form a self- trapped hole (STH). The STH can be considered as the $(AgCl_6)^{4-}$ complex with approximately 84% of the hole wavefunction density located on the central silver ion and four equatorial chlorine ions along the $\langle 100 \rangle$ directions in the plane perpendicular to the axis of the Jahn–Teller distortion. Free electrons can be captured by some Coulombic core to form shallow electron centres (SEC), which are believed to play an important role in latent image formation. A STH can capture an electron from the conduction band into a very delocalized hydrogen-like 1s orbital to form a self-trapped exciton (STE). STE, STH and SEC have been successfully studied by ODMR, electron paramagnetic resonance (EPR), ENDOR and spin-echo techniques (see [13–18] and references therein).

Pulsed ENDOR experiments have shown that the wavefunction of SEC in AgCl single crystals is very diffuse, with a Bohr radius of around 1.5 nm, and provided evidence in favour of a model of a shallowly trapped electron centre having a split-interstitial silver pair as a core [18]. Relative-energy calculations [19] support the model and demonstrate that the stable configuration for the interstitial silver ion in AgCl is likely to have the split-interstitial geometry, with this centre acting as a shallow trap for photoelectrons. It has been established by means of ENDOR that a STE in AgCl consists of a very diffuse electron (with a Bohr radius of 1.51 ± 0.06 nm) attracted by a strongly localized STH which is virtually identical to an isolated STH [20].

The effects of confinement on shallow centres with a Bohr radius comparable with the particle size are well known (see [1–3] for references). The influence of the nanoparticle size on deep-level centres and local effects in solids is of fundamental importance, but is much less studied, as far as we are aware. The Jahn–Teller (J–T) effect is one of the basic local effects in solids, and is rather sensitive to internal fields and variations of the electron–phonon interaction. STH and STE in bulk AgCl are classical J–T systems, well studied in bulk AgCl by various radiospectroscopic techniques. Therefore, investigation of AgCl nano- and microcrystal systems embedded in a crystalline matrix seems to be very interesting.

In this communication, we report on a study of STH, STE and SEC in small AgCl crystals of varied size, embedded in a KCl matrix, by optical spectroscopy and the EPR and ODMR techniques. We demonstrate the existence of impurity clusters ranging from single or paired silver ions to AgCl microcrystals retaining the properties of bulk AgCl crystals and having the same orientation as the host KCl crystal. It should be noted that the problem of identifying the AgCl microcrystals embedded in KCl was easily solved, because the EPR and ODMR spectra of microcrystals are practically the same as those of bulk AgCl and can be used as a 'fingerprint' of AgCl. By contrast, it is more difficult to discriminate between the ODMR spectra of STH, STE and SEC in AgCl nanocrystals and the spectra of Ag-related point defects in KCl. That is why the silver-related point defects in KCl:AgCl are briefly discussed. The ODMR in a reference sample of bulk AgCl crystal used for doping KCl was studied in order to test its quality and to obtain reference ODMR spectra. One of the main purposes of this work was to study the influence of the particle size on the local J–T effect in nanocrystals. A theoretical model has been developed which explains the decrease in the g-factor anisotropy experimentally observed for STH and STE, which implies the suppression of the J–T effect in AgCl nanocrystals embedded in the KCl matrix.

2. Experiment

KCl:AgCl single crystals were grown by the Stockbarger technique with 1 to 3 mol% Ag in the melt. Nominally pure AgCl crystals were used for the doping. AgCl enriched in ^{109}Ag was used in some EPR measurements. Transparent optical-quality KCl:AgCl samples were cleaved along the {100} planes. It should be noted that the easy cleavability of alkali halide crystals is the major advantage of the matrix. AgCl could be cleaved at 77 K only. Several KCl:AgCl crystals were grown and studied, but the principal results of this work were obtained with four KCl:AgCl samples cleaved from the bottom (sample No 1), top (sample No 2) and intermediate (sample No 4) regions of the same boule grown with 2 mol% silver in the melt. Sample No 3 was identical to sample No 2, but was studied two months later, after being kept in the dark at room temperature.

The X- and Q-band EPR was recorded with a commercial JEOL spectrometer equipped with a helium gas-flow cryostat. The optical absorption was measured using a double-beam spectrophotometer. The ODMR was studied with a 35 GHz ODMR spectrometer operating at 1.6 K and providing a magnetic field of up to 4.5 T. The samples were placed at the centre of a cylindrical H_{011} microwave cavity with openings for excitation and emission light. Its unloaded Q-factor exceeded 3000. The maximum microwave power in the cavity was 900 mW. Luminescence was excited with the light of a 400 W deuterium arc lamp, passed through a broad-band filter transparent in the range 260–400 nm. Microwaves were chopped at $f_{\mathrm{chop}} = 80$ Hz to 10 kHz with a p–i–n diode and the microwave-induced variations of the luminescence intensity were detected with a lock-in amplifier.

3. Experimental results

3.1. Point defects and clusters in KCl:AgCl

Under UV light or x-ray irradiation, a number of silver-related point defects can be formed in KCl:Ag crystals grown even with a small ($\leqslant$0.5 mol%) concentration of silver. One of the problems to be solved in the present study was that of how to distinguish EPR and ODMR spectra of AgCl micro- and nanocrystals in KCl from those associated with Ag-related point defects. Therefore, we studied the EPR of heavily doped KCl:AgCl crystals after x-ray irradiation and subsequent optical bleaching of certain centres by the procedures described in [9–11].

Figure 1 presents EPR spectra and models of silver-related paramagnetic centres that we observed in KCl:AgCl (2 mol%) crystals. Information concerning the electronic structure

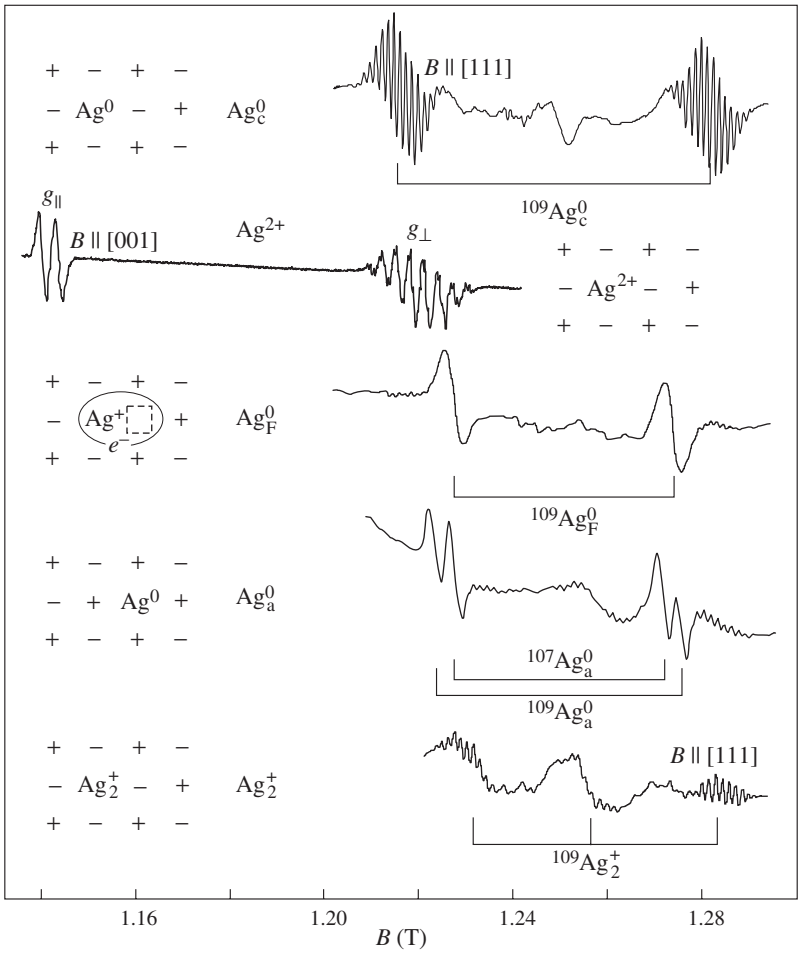

Figure 1. Simplified models and 35 GHz EPR spectra of silver-related point defects in x-ray-irradiated KCl:^{109}AgCl (2 mol%) crystals: silver atoms at the cation position Ag_c^0, hole centres Ag^{2+}, laser-active Ag_F^0 centres, silver atoms Ag_a^0 at the anion positions (in KCl:Ag with the natural silver isotope abundance) and silver pairs Ag_2^+.

and symmetry of these centres has been obtained previously [9–11] by means of a careful analysis of EPR spectra. Silver impurity ions in KCl:Ag crystals substitute for alkali ions (Ag_c^+). Ag_c^+ are both donors and acceptors and can therefore trap both electrons and holes. As a result of UV or x-ray irradiation of KCl:AgCl, an electron centre Ag_c^0—a silver atom at a cation position with no perturbing defects in the neighbourhood—and a hole centre Ag^{2+} are produced. Together with these elementary centres, a number of more complicated silver-related defects can be formed as shown in figure 1—namely, a complex of a silver atom with a nearby anion vacancy or laser-active Ag_F^0 centres, silver atoms Ag_a^0 at anion positions and silver pairs Ag_2^+. In addition, negative silver ions at an anion position, Ag_a^-, non-paramagnetic in the ground state but having a triplet excited state, can be created.

The Ag_2^+ centre is suggested to be a split-interstitial silver pair. It can be considered as a first step to forming larger AgCl clusters in KCl. It should be noted that the Ag_2^+ centre could be produced by x-ray irradiation only at temperatures above 250 K when the positive-ion vacancies are mobile. We believe that as-grown heavily doped KCl:AgCl crystals contain a large fraction of Ag_c^+–Ag_c^+ pairs. Under x-ray irradiation such pairs can capture an electron to form a Frenkel pair, i.e. one of the adjacent Ag^+ ions is displaced to an interstitial position and gives rise to a molecular centre, Ag_2^+, and a nearby cationic vacancy. When the temperature is raised to above 250 K, the positive-ion vacancies become mobile and diffuse away from the Ag_2^+ centre, which is neutral in the crystal lattice and needs no charge compensation.

The observation of well-resolved EPR spectra of the atomic-size silver-related paramagnetic centres shows the existence of dispersed single and paired silver ions in the heavily doped KCl:AgCl crystals and confirms their high crystallographic quality.

3.2. ODMR in bulk AgCl

The ODMR in the reference bulk AgCl crystal used for doping of KCl was studied in order to test its quality and to obtain reference ODMR spectra measured under the same conditions as those used to study AgCl micro- and nanocrystals. Figure 2 shows the 35 GHz ODMR in bulk AgCl recorded at $\vec{B} \parallel [100]$ as microwave-induced variations of the intensity of the total emission at two values of the microwave power: 6 mW (full curve) and 300 mW (broken curve).

Anisotropic ODMR signals of STH and STE and an isotropic line of SEC are observed, as indicated in figure 2. They correspond to the well-known ODMR in bulk AgCl crystals, which has been extensively studied (see, e.g., [13–17]). Since the STH are Jahn–Teller-distorted along one of the three ⟨100⟩ axes, three types of centre exist. The lines indicated by '$\parallel$' belong to the centres with the J–T distortion axes oriented parallel to the magnetic field $\vec{B}$, whereas the lines indicated by '$\perp$' belong to the centres with the axes perpendicular to $\vec{B}$. The same applies to the triplet state of the STE, because the central hole of the STE is virtually identical to an isolated STH. In the latter case two lines are observed for each of the possible centre orientations because of the zero-field (fine-structure) splitting. The energy schemes for STE and the corresponding transitions are shown in the upper part of figure 2. The observation of ODMR of STH and SEC implies that, in addition to the emission from STE, the recombination of distant STH–SEC pairs contributes to the luminescence of AgCl.

ODMR spectra of STE can be described by the general spin Hamiltonian

$$\hat{H} = \beta \vec{B} \cdot \hat{g}_e \cdot \vec{s}_e + \beta \vec{B} \cdot \hat{g}_h \cdot \vec{s}_h + \vec{s}_e \cdot \hat{D} \cdot \vec{s}_h + J \vec{s}_e \cdot \vec{s}_h \tag{1}$$

where β is the Bohr magneton. The first two terms are Zeeman interactions of an electron with spin $\vec{s}_h$ and a hole with spin $\vec{s}_e$, respectively. The g-tensor of the hole $\hat{g}_h$ is identical to that of the STH and has axial symmetry about one of the ⟨100⟩ axes. Since the electron is weakly

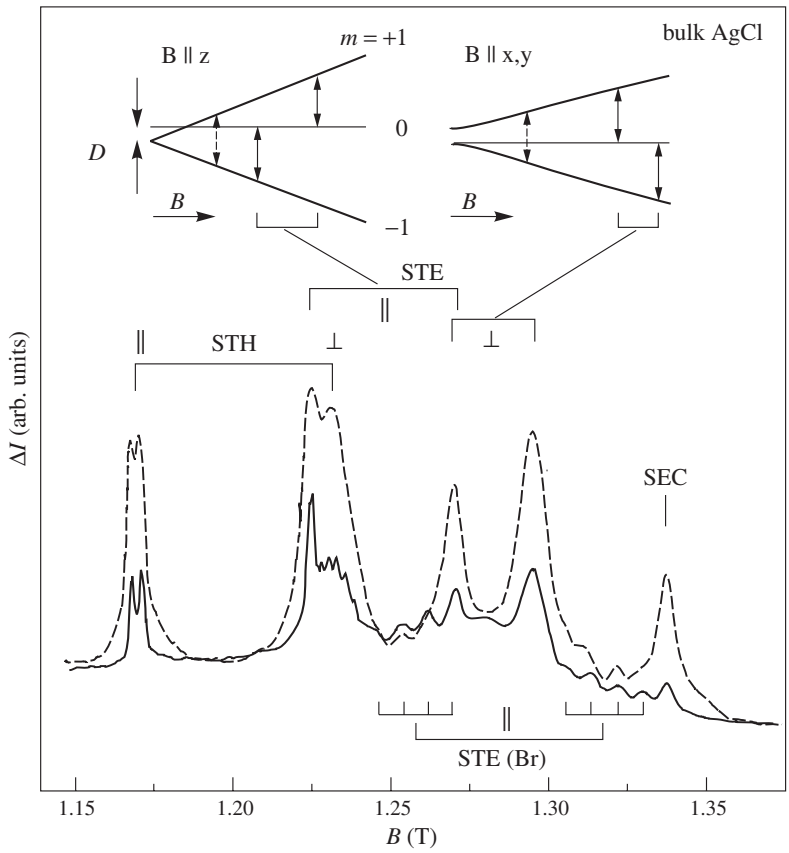

Figure 2. ODMR in the reference sample of bulk AgCl, recorded as microwave-induced variations of the total emission intensity at a microwave power of 6 mW (full curve) and 300 mW (broken curve). The energy level diagrams for the triplet state of the STE and the observed EPR transitions are shown at the top. $T = 1.6$ K; $\nu = 35.2$ GHz; $f_{\text{chop}} = 80$ Hz; $\vec{B} \parallel [001]$.

bound to the hole, the g-tensor of the electron must resemble that of a SEC and, therefore, it is isotropic ($g_e = 1.88$ for bulk AgCl). The third term in (1) represents the electron–hole spin–spin interaction, which also reflects the axial symmetry. The principal axes of the tensor $\hat{D}$ coincide with those of the g-tensor and with the $\langle 100 \rangle$ crystal axes.

The fourth term in (1) describes the isotropic exchange interaction between the electron and the hole. If this interaction is much stronger than the other terms in (1), the system is most conveniently described in terms of the total spin S. The two spins 1/2 are coupled into a singlet ($S = 0$) state and a triplet ($S = 1$) state. The energies of these total spin multiplets follow the Landé interval rule, and the splitting between the singlet and triplet states is J. For an axial $S = 1$ system, like STE in AgCl, the 35 GHz EPR and ODMR spectrum can be described by the spin Hamiltonian

$$\hat{H} = \mu_B \vec{B} \cdot \hat{g} \cdot \vec{S} + D\left[S_z^2 - \frac{1}{3}S(S+1)\right] \tag{2}$$

where the first term is the Zeeman interaction for STE and the second term describes the fine structure with a splitting D. The hyperfine (hf) structure which can be observed for STH is

not present in equations (1) and (2). The tensor $\hat{g}$ of a STE can be written as

$$\hat{g} = \frac{\hat{g}_h + \hat{g}_e}{2}. \tag{3}$$

For the principal axes, which are parallel to the ⟨100⟩ crystal axes, $g_\parallel = 0.5(g_{\parallel h} + g_e)$ and $g_\perp = 0.5(g_{\perp h} + g_e)$. The experimental parameters for STH, STE and SEC in bulk AgCl are given in table 1.

Table 1. Parameters for STH, STE and SEC in bulk AgCl crystals and AgCl micro- and nanocrystals embedded in KCl matrix.

		Centre						
		STH		STE			SEC	
Crystal		$g_\parallel$	$g_\perp$	$g_\parallel$	$g_\perp$	D (MHz)	g	References
Bulk AgCl		2.147	2.040	2.016	1.968	−710	1.881	[14, 23]
AgCl	Microcrystals	2.147	2.040	2.020	1.966	−710	1.88–1.90	This work
embedded	Nanocrystals	—	—	1.992	1.964	−335	—	[7]
in KCl	Nanocrystals	2.016	1.974	1.992	1.965	−335	∼ 1.96	This work

Since the STE in AgCl consists of a highly diffuse electron bound to a strongly localized STH, the isotropic exchange splitting J between the singlet and the triplet states is too small to observe in the optical spectra, but it can be directly measured by means of EPR and ODMR. The value of J has been estimated to be 1 to 25 cm^{-1} [14] and 6 to 7 cm^{-1} [15]. $J = -5.37 \pm 0.01$ has been measured by direct observation of the singlet-to-triplet 'forbidden' transition in 95 GHz ODMR and electron-spin-echo experiments [16]. Another way to determine J was followed in [17, 21] where multiquantum singlet-to-triplet transitions corresponding to the absorption of up to seven microwave quanta (total energy $7 \times 35 = 245$ GHz) were found in the ODMR of STE in bulk AgCl crystals. This finding allowed J to be measured with extremely high accuracy: $J = -5.370 \pm 0.002\,cm^{-1}$.

The energy level scheme of STE for $\vec{B} \parallel [100]$ and the experimentally observed multiquantum ODMR transitions for STE, STH and SEC in bulk AgCl are shown in figure 3(a). In addition to the transitions within the triplet state of the STE designated as 'STE (T)', lines are observed, corresponding to the singlet-to-triplet multiquantum transition and denoted by 'STE (S–T)'. This surprising result has been unambiguously proved by measuring the ODMR at slightly different microwave frequencies, i.e. at different energies of the microwave quanta [17]. The directions and the values of the line shifts were different for different transitions, in complete agreement with the calculations using the spin Hamiltonian (1).

The multiquantum ODMR in KCl:AgCl (figure 3(b)) will be discussed below.

Although the multiquantum ODMR has been observed by different groups in several systems, complete understanding of this effect is still lacking. One of the possible explanations of the strong multiquantum ODMR [21] takes into account multiquantum transitions via real intermediate electronic states. According to this mechanism, both the electric (E) and magnetic (H) components of the microwave field may be active in the multiquantum transitions including an effect of interference of E and H. The intermediate states may appear as a result of a vibronic interaction in a quasi-degenerate system of electronic states of the centre. The possibility of successive transitions, involving absorption of both the H- and the E-components, was demonstrated in [18]. It is not inconceivable that the intermediate states are associated with the presence of free carriers. Probably, these states are actually observed in the ODMR of AgCl as a broad background signal.

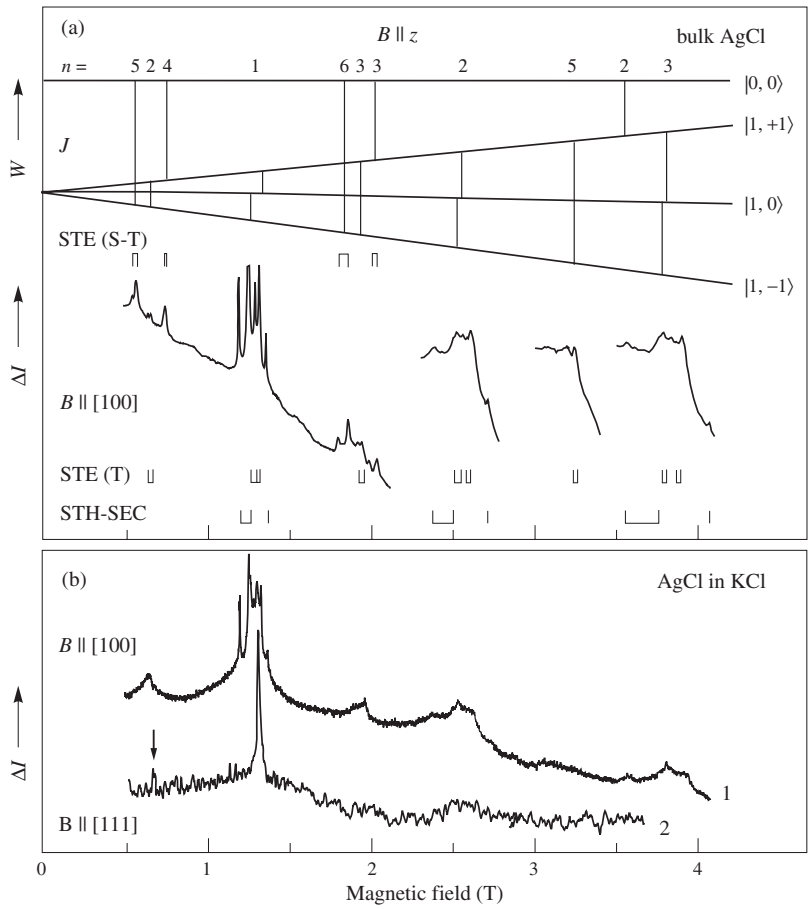

Figure 3. (a) The energy level scheme for STE with multiquantum transitions and ODMR measured at high microwave power (900 mW) in bulk AgCl and (b) the ODMR measured under the same conditions in KCl:AgCl samples Nos 1 and 2 (spectra 1 and 2 respectively). n denotes the number of microwave quanta. $T = 1.6$ K; $\nu = 35.2$ GHz; $f_{\text{chop}} = 80$ Hz.

In addition to the ODMR signals discussed above, figure 2 shows the ODMR lines denoted by STE(Br). Bromine is a common trace impurity in AgCl. As shown in [19, 23–25], a minor concentration of bromine in AgCl gives rise to an $[AgCl_5Br]^{5-}$ exciton trapped at an isolated bromine site. The cross-section for the electron–hole recombination at silver ions perturbed by bromine ligands is approximately an order of magnitude greater than that for unperturbed silver ions [23]. It was suggested that the higher stability of the hole near the bromine site is a consequence of the fact that the electronegativity of chlorine is greater than that of bromine, with the result that the holes are preferentially trapped at the bromine sites.

3.3. ODMR and luminescence in self-organized AgCl microcrystals and nanocrystals embedded in KCl crystalline matrix

Figure 4 shows luminescence (part (a)) and ODMR (part (b)) spectra recorded at 1.6 K with three KCl:AgCl samples: No 1 (luminescence and ODMR spectra 1), No 2 (spectra 2) and No 3 (spectra 3). Optical absorption measurements for these samples showed additional absorption

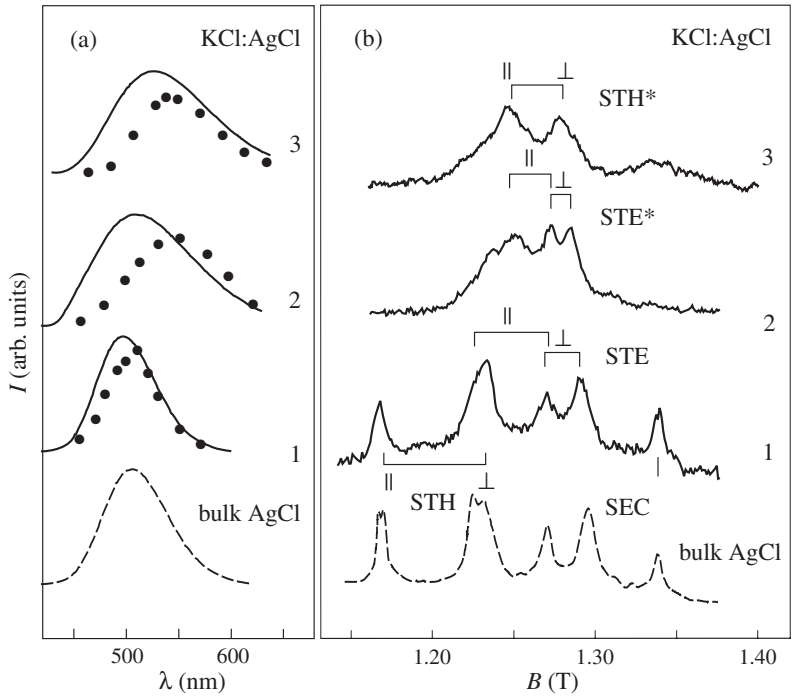

Figure 4. Luminescence (a) and ODMR (b) spectra for three samples: No 1 (luminescence and ODMR spectra 1), No 2 (spectra 2) and No 3 (spectra 3) of KCl:AgCl grown with 2 mol% Ag in the melt. Points in (a) show the spectral dependences of the ODMR signals. For comparison, the luminescence and ODMR spectra for bulk AgCl are shown by broken curves in the lower part of the figure. The positions of the ODMR lines are marked for STE, STH and SEC in AgCl microcrystals and AgCl nanocrystals (STE* and STH*). Symbols ∥ and ⊥ denote the centres with axes parallel and perpendicular to the magnetic field. $T = 1.6$ K; $\nu = 35.2$ GHz; $P = 300$ mW; $f_{\text{chop}} = 80$ Hz; $\vec{B} \parallel [001]$.

at a wavelength corresponding to the band gap of AgCl. The luminescence and ODMR spectra of bulk AgCl, taken under the same conditions, are shown for comparison in the lower part of the figure by a broken curve. Points in figure 4(a) represent the spectral dependences of the ODMR amplitude.

A striking result is the remarkable similarity of the ODMR spectra recorded for KCl:AgCl sample No 1 and for the bulk AgCl crystal. The spectral dependence of the ODMR in sample No 1 is also close to the luminescence spectrum of bulk AgCl (figure 1(a), spectrum 1). The ODMR spectrum 1 is practically identical to that of bulk AgCl but the ODMR lines are somewhat broadened. The principal axes of STH and STE coincide with the ⟨100⟩ axes of KCl, which indicates that the AgCl crystals in KCl retain the symmetry of the matrix. We ascribe the ODMR observed in sample No 1 to micrometre-size AgCl crystals (microcrystals) embedded in the KCl matrix. Similar ODMR spectra with the same parameters for STH and STE were recorded for several KCl:AgCl crystals. In some samples the line for SEC was shifted downfield and slightly broadened. This means an increase in the g-factor and a distribution of its values. The parameters for STH, STE and SEC in AgCl microcrystals, obtained by analysing the angular dependences of ODMR, are listed in table 1.

The ODMR spectra 2 and 3 in figure 4(b) exhibit lines of the triplet ($S = 1$) and doublet ($S = 1/2$) states. Spectrum 2 contains ODMR lines which are marked in the figure and can

be attributed to the triplet state. This conclusion was confirmed by an analysis of the angular dependences in the (110) and (100) planes and by observation of the forbidden $\Delta m = 2$ transitions seen in figure 3(b) at ≈0.65 T. The parameters of the triplet obtained by fitting the angular dependences and the spin Hamiltonian (2) are the same as those of the ODMR spectra ascribed in [7] to STE in AgCl nanocrystals embedded in a KCl matrix. We denote these spectra by STE*. According to data furnished by atomic force microscopy [7], the average size of the AgCl nanocrystals is 5–7 nm. The ODMR lines of the $S = 1/2$ state, ascribed to STH in AgCl nanocrystals (STH*), are better resolved in the ODMR of sample No 3 (figure 4(b), spectrum 3).

The lines for STH, STE and SEC in the 35 GHz ODMR spectra of sample No 1 and bulk AgCl are well resolved owing to the strong anisotropy of the g-factors and relatively large fine-structure splitting D. For the ODMR of $S = 1/2$ and $S = 1$ centres in samples Nos 2 and 3, both the anisotropy of the g-factors and the parameter D are considerably reduced. Nevertheless, we were able to discriminate between the signals of the $S = 1$ and $S = 1/2$ centres, since the relative intensities of the ODMR spectra depend on the microwave power and the chopping frequency. The angular variations of the ODMR in sample No 2 for a rotation of the magnetic field in the (110) plane are shown in figure 5. Full and broken curves represent the ODMR spectra recorded with chopping frequencies of 80 Hz and 800 Hz, respectively. The signals of the doublet spectrum are more pronounced at higher chopping frequencies.

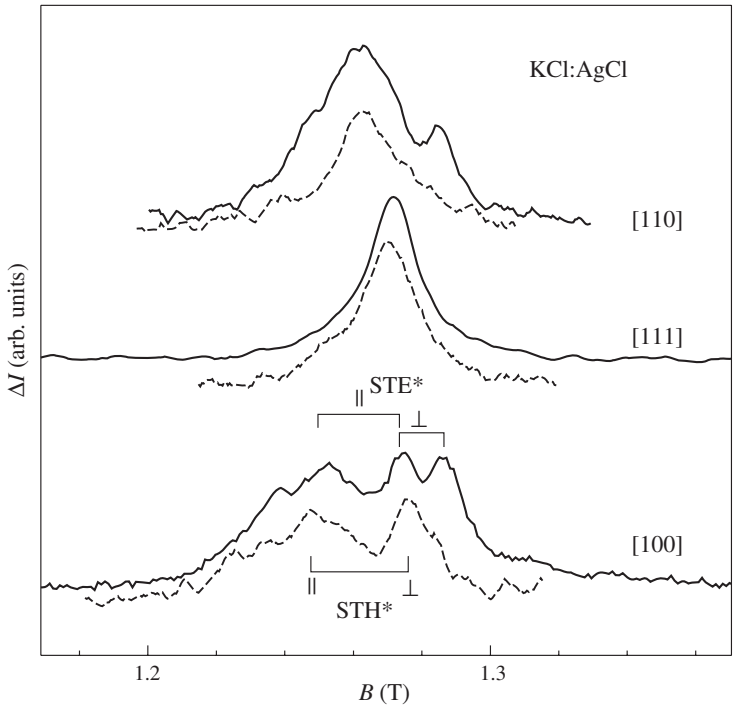

Figure 5. ODMR in KCl:AgCl sample No 2 recorded with $f_{chop} = 80$ Hz (full curves) and $f_{chop} = 800$ Hz (broken curves) for the three principal orientations in the (110) plane. $T = 1.6$ K; $\nu = 35.2$ GHz; $P = 300$ mW.

On the other hand, the relative intensities of the $S = 1/2$ and $S = 1$ ODMR depend on the history of a sample. It can be seen from figure 4(b), spectra 3 and 4, that the relative amplitude of the $S = 1/2$ spectrum increases upon storing the sample in the dark for two

months. In addition, new broad lines appear in the ODMR spectrum 4. The angular variations of the ODMR in sample No 3 with a dominant $S = 1/2$ spectrum are displayed in figure 6 for the case of rotation in the (100) plane. The parameters of the ODMR spectra ascribed to STE and STH in AgCl nanocrystals (STE* and STH*) are listed in table 1. They are substantially different from those for AgCl microcrystals and bulk AgCl. D is taken to be negative by analogy with bulk AgCl, although in our measurements, as also in [7], there is no direct experimental evidence of the sign of D.

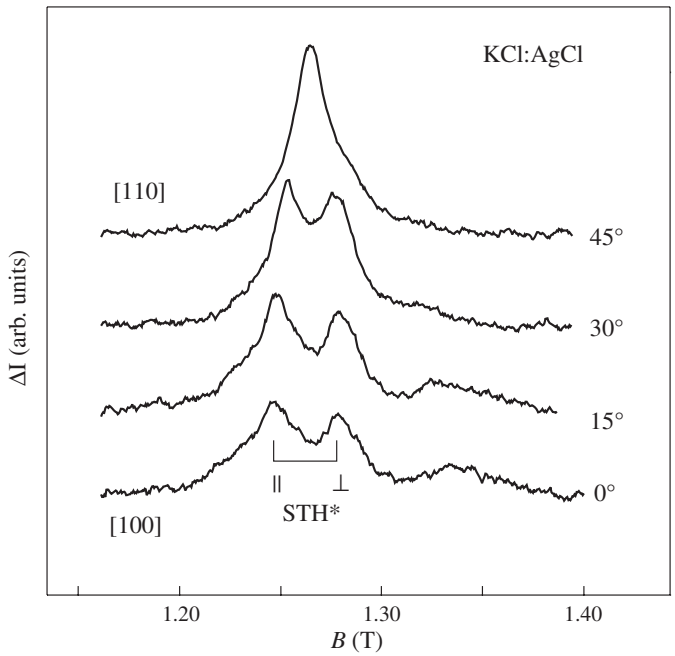

Figure 6. Angular variations of the ODMR in KCl:AgCl sample No 3 for a rotation of the magnetic field in the (100) plane. The angle is marked between the magnetic field and the [100] axis. $T = 1.6$ K; $\nu = 35.2$ GHz; $P = 100$ mW; $f_{\text{chop}} = 80$ Hz.

The difference between the luminescence and ODMR spectra of samples No 1 and Nos 2, 3 seems to be associated with a decrease in the average size of the embedded AgCl crystals from micrometre to nanometre scale. The ODMR spectrum of sample No 4 cleaved from the intermediate region between samples Nos 1 and 2 is a superposition of the of micro- and nanocrystal ODMR spectra. This confirms the coexistence of micro- and nanocrystals in this sample. The ODMR spectra recorded from sample No 4 with spectral resolution are displayed in figure 7. The inset shows a luminescence spectrum and the wavelengths at which the ODMR spectra were measured. With the wavelength increasing from 490 to 540 nm, the ODMR signals from AgCl microcrystals disappear and the ODMR spectra of AgCl nanocrystals become more intense, in agreement with the spectral dependences of the ODMR for AgCl micro- and nanocrystals shown in figure 4(a), spectra 1 and 2, for samples Nos 1 and 2, respectively. It should be emphasized that no smooth transition from a 'bulk-like' ODMR to a 'nanocrystal' ODMR was observed.

The ODMR spectra recorded at high microwave power with the AgCl microcrystals (KCl:AgCl, sample No 1) and nanocrystals (sample No 2) are shown in figure 3(b). It should be noted that the exchange splitting J of STE can serve as a measure of the spatial extent of

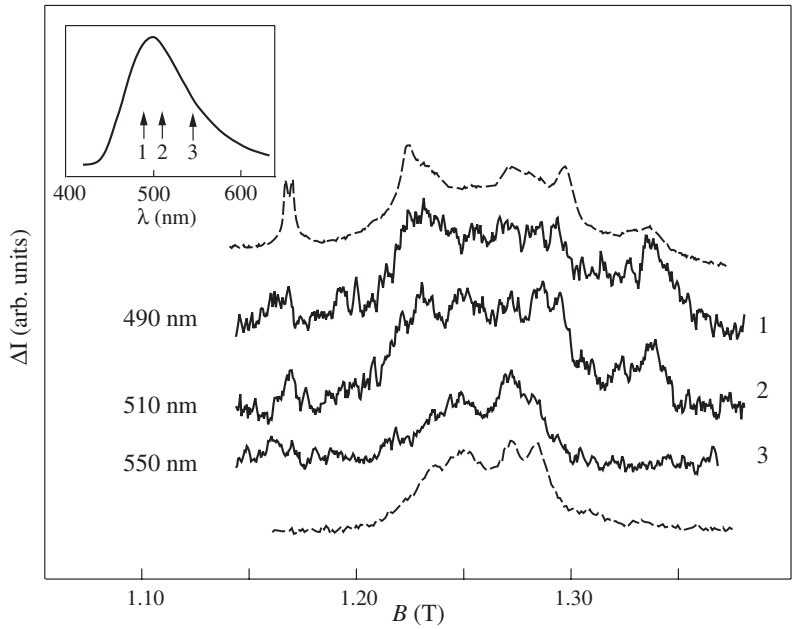

Figure 7. Luminescence (inset) and ODMR spectra of KCl:AgCl sample No 4, measured with spectral resolution at the wavelengths marked in the inset. ODMR spectra of AgCl micro- and nanocrystals are shown by broken curves in the upper and lower parts of the figure for comparison. $T = 1.6$ K; $\nu = 35.2$ GHz; $P = 300$ mW; $f_{\text{chop}} = 80$ Hz; $\vec{B} \parallel [001]$.

the electron wavefunction and can provide information about the confinement effects for SEC and STE due to the nanocrystal size. The confinement of the wavefunction in nanocrystals is also believed to affect the g-factor shift of SEC. We did observe a shift and a broadening of the ODMR line of SEC for some KCl:AgCl samples exhibiting a bulk-like ODMR. In sample No 1, we observed multiquantum transitions related to STH and SEC, and those within the triplet state of STE, similarly to the case for bulk AgCl, but no singlet-to-triplet transitions were detected (figure 3(b), spectrum 1). This may imply a different (larger) value of the singlet–triplet splitting. In sample No 2, multiquantum transitions were much weaker and were seen only in the field range corresponding to $g = 1$ (figure 3(b), spectrum 2).

It should be noted that there exists a correlation between the observation of a multiquantum ODMR and the so-called non-resonant background believed to be associated with the action of the electric component of the microwave field on free carriers: the stronger the background, the more pronounced the multiquantum ODMR. Similar effects have been observed in multiquantum ODMR in semiconductors [12]. A rather strong non-resonant background was observed in bulk AgCl, corresponding to enhancement of the emission intensity by microwaves and having a smooth dependence on magnetic field. The background was weaker for AgCl microcrystals (sample No 1) and very weak for AgCl nanocrystals (sample No 2).

The luminescence and ODMR spectra of KCl:AgCl change upon keeping the samples in the dark at room temperature and also upon thermal treatment. The increase in the relative intensity of ODMR signals of STH* for sample No 3 (i.e. for sample No 2 after two months of storage in the dark) implies a change of the recombination processes in nanocrystals during relaxation.

The positions of broad anisotropic lines appearing in the ODMR of sample No 3 (see figure 6) can be described by $S = 1$, $g_{\|} = 1.95$, $D = 28$ mT and seem to correspond to the ODMR of $[AgCl_5Br]^{5-}$ excitons probably present in AgCl nanocrystals. No bromine hyperfine structure was resolved. We believe that the corresponding centre has a practically tetragonal symmetry, but our measurements did not demonstrate this conclusively because of the difficulty in constructing detailed angular plots.

4. Discussion and theoretical consideration

4.1. General

In the present study, three types of ODMR spectrum were observed for heavily doped KCl:AgCl, relating to the following centres presented in table 1:

(i) STH, STE and SEC in oriented AgCl microcrystals, having parameters close to those of bulk AgCl.
(ii) Anisotropic centres with $S = 1/2$ and $S = 1$ ascribed to STH and STE in AgCl nanocrystals and having parameters essentially different from those of bulk AgCl.
(iii) Centres apparently present in AgCl nanocrystals, with parameters close to those of the triplet Br-related $[AgCl_5Br]^{5-}$ excitons.

Observation of bulk-like ODMR in KCl:AgCl can be considered the first direct confirmation of the formation of AgCl microcrystals (apparently of micrometre size) in the KCl matrix. These microcrystals have practically the same properties as bulk AgCl and retain the orientation of the host KCl lattice. The misorientation of the AgCl microcrystals, estimated from the ODMR spectra, is below 5°. Thus, the ODMR spectra were used as a fingerprint of the embedded AgCl crystals and a confirmation of their high crystallographic quality.

Although the arguments in favour of the assignment of the ODMR spectra of samples Nos 2 and 3 to AgCl nanocrystals seem to be rather convincing, the possibility that they may be associated with point defects in KCl should not be ruled out. Our analysis of the EPR and ODMR spectra showed that the ODMR spectra obtained do not correspond to EPR of any known point defect or STE in KCl.

As follows from equation (3), there exists a direct link between the g-factors of STE and those of STH and SEC. This strictly holds for bulk AgCl crystals and AgCl microcrystals (see table 1). It is natural to suppose that the same is valid for the AgCl nanocrystals. It is seen from table 1 that the g-factors for STH* and STE* in AgCl nanocrystals satisfy equation (3) within experimental error if we suppose that the g-factor of SEC remains isotropic in the nanocrystals. In addition, this allows us to estimate the g-factor of SEC in AgCl nanocrystals to be $\approx$1.96, which greatly exceeds the bulk AgCl value. No ODMR of SEC in nanocrystals was definitely detected, probably owing to its possible overlap with the stronger signals of STE* and STH* and broadening of the ODMR line because of the nanocrystal size distribution. We emphasize that the correlation between the g-factors of the $S = 1/2$ and $S = 1$ centres strongly supports their identification as STH and STE in AgCl nanocrystals. Such arguments have been lacking previously.

The triplet ODMR spectra (figures 4 and 5) have the same parameters as the ODMR measured in [7] in KCl:AgCl where AgCl nanocrystals with the average size of 5–7 nm were directly observed by atomic force microscopy. Thus, the results of our work, together with those of reference [7], suggest that impurity clusters ranging from single and paired Ag ions to AgCl nanocrystals and larger micrometre-size microcrystals exist in heavily doped KCl:AgCl. In AgCl microcrystals, the properties of STH and STE are similar to those of bulk AgCl,

and only slight deviations of the g-factor of SEC are detected—namely, the g-factor shift $\Delta = g_e - g_{SEC}$ decreases and a certain dispersion of g-factors leading to ODMR broadening is observed in some samples.

One of the important results is that the ODMR spectra of KCl:AgCl vary with time of sample storage in the dark at room temperature. Changes over long timescales were observed in both the luminescence and ODMR spectra of AgCl nanocrystals, i.e. the recombination processes in AgCl nanocrystals varied with time. Thus, the as-grown AgCl crystals embedded in the KCl matrix are metastable and their relaxation into the stable state seems to require months. This implies that the crystals are in a metastable state after growth and they need months to relax into the ground state. Similar 'ageing' effects were observed in [5] for CuCl nanocrystals embedded in an alkali halide matrix. The existence of deformation fields around the nanocrystals embedded in alkali halides was demonstrated for CuCl nanocrystals by scanning near-field microscopy [25].

In AgCl nanocrystals of size as small as 10 nm, both the doublet and the triplet ODMR spectra ascribed to STH and STE were found, with parameters essentially different from those of STH and STE in bulk AgCl. It can be seen from table 1 that a considerable decrease in the g-factor anisotropy is observed both for isolated STH and for STH forming STE in the AgCl nanocrystals embedded in the KCl matrix. In bulk AgCl crystals the difference $g_\parallel - g_\perp$ is 0.107 for STH and 0.054 for STE. In AgCl nanocrystals the respective values are 0.042 and 0.027, i.e. approximately two times smaller. Such a strong decrease in anisotropy requires an explanation, which is the subject of the following subsection.

4.2. Theoretical consideration of the suppression of the Jahn–Teller effect in nanoparticles

Ag^{2+} ions have a $4d^9$ electronic configuration. In an octahedral environment the fivefold orbitally degenerate ^2D ground state is split into a triplet $^2T_{2g}$ and a doublet ^2E_g. Further tetragonal distortion produces an extra splitting of the doublet into two singlets ($^2A_1$ and $^2B_1$ if the point symmetry is C_{4v}) corresponding to the unpaired electron wavefunctions θ and ε that span the doublet ^2E_g and transform, respectively, like $(3z^2 - r^2)$ and $(\sqrt{3})(x^2 - y^2)$ under the operation of the cubic group. Which of the singlets has lower energy depends on the type of the tetragonal distortion involved. If the two orbital states are well separated, the lower singlet with its twofold spin degeneracy will behave in a first approximation like a spin doublet. However, the spin–orbit coupling mixes some of the states of the triplet $^2T_{2g}$ into the ground state, making the g-values different from the free-spin value and introducing some anisotropy.

In the case of an unpaired electron in the low-symmetry field we have [26]: $g_\parallel = 2 - 8\lambda/\Delta_0$, $g_\perp = 2 - 2\lambda/\Delta_1$ for the ε-orbital; and $g_\parallel = 2$, $g_\perp = 2 - 6\lambda/\Delta_2$ for the θ-orbital. Here λ is the spin–orbit coupling constant ($\lambda < 0$ for Ag^{2+}) and Δ_0, Δ_1 and Δ_2 are the following orbital energy differences:

$$\Delta_0 = \left|E_{4d(xy)} - E_{4d(x^2-y^2)}\right|$$

$$\Delta_1 = \left|E_{4d(xz),4d(yz)} - E_{4d(x^2-y^2)}\right|$$

$$\Delta_2 = \left|E_{4d(xz),4d(yz)} - E_{4d(z^2)}\right|.$$

Since $|\lambda| \ll \Delta_1, \Delta_2, \Delta_3$, we have $g_\parallel > g_\perp > 2$ if the ground state is the ε-orbital and $g_\perp > g_\parallel \cong 2$ if the ground state is θ. It follows from experiment (table 1) that the ground state of Ag^{2+} centres is the ε-orbital. This orbital has its four lobes pointing towards four chlorine nuclei located in a plane perpendicular to the tetragonal axis.

The anisotropy of the g-factor of the ^{2}E J–T state of STH in the cubic environment is determined by the effective Zeeman interaction in the form [27]

$$\hat{Z} = g_1\beta\vec{B}\cdot\vec{S} + \frac{g_2\beta}{2}[(3B_zS_z - \vec{B}\cdot\vec{S})\hat{U}_\theta + \sqrt{3}(B_xS_y - B_yS_x)\hat{U}_\varepsilon] \tag{4}$$

where: $g_1 = g_s - (4\lambda/\Delta)$; $g_2 = -(4\lambda/\Delta)$; $\Delta = 10Dq$ (in the zero approximation, $\Delta_1 \approx \Delta_2 \approx \Delta_0 \approx \Delta$); and $\hat{U}_\varepsilon$ are the corresponding electronic operators on the basis of the ^{2}E state:

$$\hat{U}_\theta = \frac{1}{6}[3\hat{L}_z^2 - L(L+1)] \qquad \hat{U}_\varepsilon = \frac{\sqrt{3}}{6}[\hat{L}_x^2 - \hat{L}_y^2].$$

Here $\hat{L}_x$, $\hat{L}_y$ and $\hat{L}_z$ are the components of the orbital momentum in the D state. g_1 and g_2 can be found directly from the values of $g_\parallel^{(\theta)}$, $g_\perp^{(\theta)}$ and $g_\parallel^{(\varepsilon)}$, $g_\perp^{(\varepsilon)}$ which are the values of $g_\parallel$ and $g_\perp$ in the tetragonal symmetry with either θ or ε as the non-degenerate ground level:

$$g_\parallel^{(\theta)} = g_1 - g_2 \qquad g_\parallel^{(\varepsilon)} = g_1 + g_2$$

$$g_\perp^{(\theta)} = g_1 + g_2/2 \qquad g_\perp^{(\varepsilon)} = g_1 - g_2/2.$$

As mentioned above, the ground state of STH corresponds to the ε-state.

As follows from (4), the average value of the g-factor tends to the isotropic contribution g_1 with decreasing strength of the J–T effect because $\langle\hat{U}_\theta\rangle \to 0$ and $\langle\hat{U}_\varepsilon\rangle \to 0$. Thus, the observed pronounced decrease in the g-factor anisotropy of STH in AgCl nanocrystals implies a considerable suppression of the J–T effect.

(1) Let us consider the influence of the nanocrystal size on the J–T effect for STH inside a AgCl nanocrystal embedded in the KCl matrix. Owing to partial localization of STH at the Ag^+ ion, its $4d^9$ doubly degenerate ^{2}E state interacts linearly with e distortions of the cubic environment, which results in the E × e J–T effect.

In sufficiently large 3D AgCl crystals, in which the effect of boundaries can be neglected, the main contribution to the E × e vibronic interaction comes from the e_c deformations of the $(AgCl_6)^{4-}$ cluster with the corresponding frequency ω_c of a quasi-local e vibration. This vibration is due to the essential contribution of short-wavelength phonons having high density.

In small 3D AgCl crystals there appears, however, another source of high-density oscillations, which are also active in the E × e vibronic interaction. These are long-wavelength vibrations of nanocrystals with wavelength $\lambda_c \approx 2L$, where L is the nanocrystal size. Such an e_{nano} vibration has nodules at the crystal boundaries and shows e symmetry under the conditions of conservation of the cubic symmetry of the nanocrystal. This does not contradict the results of magnetic resonance studies and may be due to the self-organization of the nanocrystal structure. The resulting E × (e + e_{nano}) vibronic interaction enhances the J–T effect.

(2) There are, however, other effective mechanisms reducing the J–T effect in nanocrystals. The first of these is associated with additional 'image' fields of the Coulomb and elastic fields of STH. These image fields interact with the electron states of the holes which have induced them. As a result, the quadratic vibronic interaction of STH with the polarization produced by the electric image field E_0, and also the linear vibronic interaction with the J–T elastic image deformation δ_0, lift the degeneracy of the ^{2}E state of STH. The corresponding splitting Δ is given by

$$\Delta = AE_0^2 + B\delta_0 \tag{5}$$

where the parameters A and B have vibronic nature. Note that the magnitude of the elastic image field δ_0 should be found self-consistently within the solution of the same complete J–T problem. On the basis of such an approach, we can conclude that the total self-consistent deformation $[(e + e_{nano}) + \delta_0]$ is suppressed by the effect of the electric image field. The second 'J–T-elastic' term in (3) leads to some increase in the strength of the J–T effect. The first 'electric image field' term converts the J–T effect into a pseudo-J–T effect, the latter being suppressed, with increasing electric image field, as AE_0^2. The suppression criterion is as follows:

$$AE_0^2\mu\omega_-^2 \geqslant (V_E^{eff})^2 \tag{6}$$

where: ω_- is the differential frequency of the bilinearly interacting coupled vibrations of the $(AgCl_6)^{4-}$ cluster e_c and of the nanocrystal e_{nano}; μ is the corresponding mass coefficient; and V_E^{eff} is the effective parameter of the vibronic interaction for the E state of STH with the above-mentioned differential vibration.

The electric image field of STH decreases as $1/r^2$, which results in $E_0^2 \propto 1/L^4$. Keeping these dependences in mind and using equations (5) and (6), we conclude that the pseudo-J–T effect will be suppressed for sufficiently small AgCl nanocrystals only. This statement is in agreement with the experimental observations.

(3) Qualitative comparison of the two competing mechanisms shows, however, that neither of them is as strong as the third one, which we now discuss. We consider variations of the electron and hole energy states at interfaces between AgCl nanocrystals and the matrix. Let us suppose, to begin with, that the nanocrystals have the shape of plates, i.e. their dimensions in one direction, $L_\parallel$, are much smaller than those in the other two orthogonal directions. We show below that this assumption is not too rigid and that the effect under consideration persists even in the case of very small anisotropy of the nanocrystal shape.

It is to be noted that the difference of the energy gaps of KCl and AgCl is as large as 5 eV and such a change in the electron splitting occurs at a distance $\Delta L \approx a$, where $a \approx 0.3$ nm is the average lattice constant. This results in a large value of the parameter W of the interface vibronic interaction, $W \approx 17$ eV nm^{-1}. The corresponding contribution of the interface to the potential energy of a nanocrystal, U_{int}, is given by

$$\Delta U_{int} = \frac{3}{2} W \frac{\Delta L}{L_\parallel} U \tag{7}$$

where U is the quasi-uniform active displacement of the lattice. We shall consider a quasi-uniform tetragonal displacement. Such a deformation of the nanocrystal results in a splitting of the hole E state, which corresponds to a transition from the J–T effect to the pseudo-J–T effect. The elastic part of the potential energy associated with the U-vibrations can be written as

$$\Delta U_{elastic} = \frac{K_0}{2} U^2 \tag{8}$$

where K_0 is the elastic parameter of this vibration. By minimizing the sum of (7) and (8) with respect to U we obtain the equilibrium displacement U_{eq} of the nanocrystal lattice:

$$U_{eq} = -\frac{3}{2}\frac{W}{K_0}\frac{\Delta L}{L_\parallel}. \tag{9}$$

The splitting of the E state of STH, appearing as a result of this equilibrium tetrahedral distortion, is given by

$$\Delta = 3\,|W V_E|\,\frac{\Delta L}{K_0 L_\parallel}. \tag{10}$$

It should be noted that $\Delta \propto L^{-1}$, i.e. the dependence on the nanocrystal size is smooth, compared with that associated with the mechanisms discussed above. Using the criterion of suppression of the pseudo-J–T effect $\Delta\mu\,\omega_-^2 \geqslant (V_{\mathrm{E}}^{\mathrm{eff}})^2$, we obtain the critical size L_{c} of the nanocrystal:

$$L_{\mathrm{c}} = 3\,|W V_{\mathrm{E}}|\,\frac{\Delta L\,\mu\omega_-^2}{K_0 (V_{\mathrm{E}}^{\mathrm{eff}})^2}. \tag{11}$$

The pseudo-J–T effect occurs in crystals with $L_\parallel > L_{\mathrm{c}}$, being suppressed in smaller nanocrystals ($L_\parallel < L_{\mathrm{c}}$).

It should be emphasized that the considerable difference between the lattice constants of AgCl and KCl crystals is one, but not the only, contribution to the interfacial effect under consideration. Actually, we take into consideration, in addition to the purely elastic field induced by the lattice mismatch, the 'mismatch' of the electronic states, corresponding to a strong modification of the electronic states at the interface. This results in the electronic mechanism of the appearance of the interfacial field. The two interfacial effects can be simultaneously accounted for by renormalization of the parameter W within the purely vibronic mechanism treated above.

Our consideration is based on the assumption that the shape of the AgCl nanocrystals is essentially non-cubic, i.e. their thickness in the direction of the tetragonal deformation is supposed to be much smaller than the dimensions in the perpendicular plane. This fact has no influence on the effects of short-range interactions associated with the closest neighbours of the STH, which mainly determine the symmetry of the spin Hamiltonian in the absence of the J–T effect. Nevertheless, the J–T effect may be rather sensitive to the long-range interaction with the interfacial field of the nanocrystal.

Now we discuss a more general situation where the dimensions of the AgCl nanocrystals, L_x, L_y and, L_z, in the three orthogonal directions are comparable. Suppose that $L_x \approx L_y \geqslant L_z = L_\parallel$. Let us take into consideration the effect of vibronic interaction of the same type as in equation (10), but with the complete spectrum of quasi-acoustic phonons of the nanocrystal. Now this interaction accounts not only for the quasi-homogeneous deformation, but also for the deformations in the wavenumber ranges $(\pi/L_\parallel) < k_z < (\pi/a)$, $(\pi/L_x) < k_x < (\pi/a)$ $(\pi/L_y) < k_y < (\pi/a)$, where a is the lattice constant. Equations (10) and (11), derived above for the 'plate-shaped' nanocrystals and only one quasi-homogeneous mode, remain valid upon the replacement

$$\frac{W}{K_0}\frac{\Delta L}{L_\parallel} \Longrightarrow \frac{2\tilde{W}a}{\pi\mu_0 V^2}\frac{\Delta L}{(L L_\perp^2)^{1/3}}\ln\left(\frac{L_\parallel}{L_\perp}\right) \tag{12}$$

where: μ_0 and V are the mass coefficient and the average sound velocity of the quasi-acoustic phonons in the nanocrystal; $\tilde{W}$ is the parameter of the linear vibronic interaction of the electron states at the interface with the tensor of deformations corresponding to the quasi-acoustic phonons; $L_\perp = L_x \approx L_y$.

It can be seen that the effect of the nanocrystal shape anisotropy has a rather smooth logarithmic-type dependence on the ratio of the nanocrystal dimensions. However, there is no reduction of the J–T effect in the case of cubic nanocrystals ($L = L_\perp$).

Thus, for sufficiently small AgCl nanocrystals the vibronic effect of the interface results in a considerable reduction or suppression of the pseudo-J–T effect. This suggests a considerable reduction or suppression of the anisotropy of the EPR spectrum of STH, i.e. a smaller difference between $g_\parallel$ and $g_\perp$.

Our estimates show that the mechanism considered can account for the reduction of the J–T effect of STH for $L < 10$ nm, which seems to be reasonable for the system under

study. In particular, at $\omega_- \approx (1/3)\omega_D$, where ω_D is the Debye frequency, $\tilde{W} = 5$ eV, $V_E^{eff} \approx V_E = 10\ \mathrm{eV\,nm^{-1}}$, $a = 0.3$ nm, $\Delta L = 0.6$ nm and $L_x \approx L_y = L_\perp = 12.5$ nm, the critical nanocrystal size in the z-direction is $L_\parallel \approx 9.6$ nm. An estimate of the critical size of $\approx$10 nm remains valid even for $|(L_\perp - L_\parallel)/L_\parallel| \approx 0.1$, which follows from the logarithmic-type dependence in (10).

It should be noted that the proposed mechanism of formation of the internal nanostructure strain field by the interface vibronic effect is rather general and is valid for a number of nanostructures and thin films.

5. Conclusions

The STH, STE and SEC in AgCl microcrystals and nanocrystals embedded in a KCl matrix and retaining the orientation of the host lattice were detected by means of ODMR. For the first time it was unambiguously shown that self-organized microcrystalline silver halides can be grown inside alkali halide crystals with the properties of bulk AgCl. AgCl microcrystals embedded in KCl could be easily identified because the ODMR spectra of the embedded microcrystals were practically the same as those of bulk AgCl and could be used as a 'fingerprint' of AgCl.

The ODMR spectra with $S = 1/2$ and $S = 1$, having smaller anisotropy compared with those of bulk AgCl and AgCl microcrystals embedded in the KCl matrix, can be most easily understood if they are assigned to STH and STE, respectively, in AgCl nanocrystals embedded in the KCl matrix. The reduced anisotropy of the g-factor both for isolated STH and for STH forming STE in AgCl nanocrystals with an average size of 5–7 nm implies a considerable suppression of the J–T effect in nano-objects.

A mechanism taking into account the additional deformation field appearing in a nanocrystal owing to a strong vibronic interaction at the interface was developed. It allows evaluation of the critical size L_c of the embedded AgCl nanocrystals at which the suppression of the Jahn–Teller effect has its onset. $L_c \approx 10$ nm in agreement with experiment. The proposed mechanism of formation of the internal nanostructure strain field through the interfacial vibronic effect is rather general and is valid for a number of nanostructures and thin films.

Finally, it is obvious that the KCl:AgCl system is very promising as regards the investigation of spatial confinement effects in nanocrystals since it furnishes an opportunity to study oriented nanocrystals in a transparent crystalline matrix and to apply such powerful techniques as ODMR and ENDOR spectroscopy to analysis of variations in the parameters of STE, STH and SEC, well known for bulk silver halides.

Acknowledgments

We are indebted to A G Badalyan for collaboration and fruitful discussions. This work was supported in part by the Russian Foundation for Basic Research (grant 00-02-16950) and the Russian programme the 'Physics of Solid State Nanostructures' (grant 99-3012)

References

[1] Bimberg D, Grundmann M and Ledentsov N N 1999 *Quantum Dot Heterostructures* (New York: Wiley)
[2] Bányai L and Koch S W 1993 *Semiconductor Quantum Dots (World Scientific Series on Atomic, Molecular and Optical Physics vol 2)* (Singapore: World Scientific)
[3] Woggon U 1997 *Semiconductor Quantum Dots (Springer Tracts in Modern Physics)* (Berlin: Springer) p 136
[4] Fröhlich D, Haselhoff M, Reimann K and Itoh T 1995 *Solid State Commun.* **94** 189
[5] Haselhoff M and Weber H-J 1998 *Phys. Rev.* B **58** 5052

[6] Stolz H, Vogelsang H and von der Osten W 1997 *Handbook of Optical Properties: Optics of Small Particles, Interfaces, and Surfaces* vol 2 (Boca Raton, FL: Chemical Rubber Company Press) p 31
[7] Vogelsang H, Husberg O, Köhler U, von der Osten W and Marchetti A P 2000 *Phys. Rev.* B **61** 1847
[8] Romanov N G, Babunts R A, Badalyan A G, Khramtsov V A and Baranov P G 2000 *Proc. 8th Int. Symp. on Nanostructures: Physics and Technology (St Petersburg)* p 308
[9] Delbecq C J, Hayes W, O'Brien M C M and Yuster P H 1967 *Proc. R. Soc.* A **271** 243
[10] Melnikov N I, Baranov P G and Zhitnikov R A 1971 *Phys. Status Solidi* b **46** K73
Melnikov N I, Baranov P G and Zhitnikov R A 1973 *Phys. Status Solidi* b **59** K111
[11] Badalyan A G, Baranov P G and Zhitnikov R A 1977 *Sov. Phys.–Solid State* **19** 1079
Badalyan A G, Baranov P G and Zhitnikov R A 1977 *Sov. Phys.–Solid State* **19** 2089
[12] Kanzaki H 1980 *Photogr. Sci. Eng.* **24** 219
[13] Hayes W and Owen I B 1976 *J. Phys. C: Solid State Phys.* **9** L69
[14] Marchetti A P and Tinti D S 1981 *Phys. Rev.* B **24** 7361
[15] Yoshika H, Sigumoto N and Yamada M 1985 *J. Phys. Soc. Japan* **54** 3990
[16] Donckers M C J M, Poluektov O G, Schmidt J and Baranov P G 1992 *Phys. Rev.* B **45** 13 061
Poluektov O G, Donckers M C J M, Baranov P G and Schmidt J 1993 *Phys. Rev.* B **47** 10 226
[17] Romanov N G and Baranov P G 1994 *Semicond. Sci. Technol.* **9** 1080
[18] Bennebroek M T, Poluektov O G, Zakrzewski A J, Baranov P G and Schmidt J 1995 *Phys. Rev. Lett.* **74** 442
Bennebroek M T, Arnold A, Poluektov O G, Baranov P G and Schmidt J 1996 *Phys. Rev.* B **54** 11 276
[19] Baetzold R C and Eachus R S 1995 *J. Phys.: Condens. Matter* **7** 3991
[20] Bennebroek M T, Arnold A, Poluektov O G, Baranov P G and Schmidt J 1996 *Phys. Rev.* B **53** 15 607
[21] Baranov P G, Romanov N G and Vikhnin V S 1992 *26th AMPERE Congr. on Magnetic Resonance (Athens, 1992)* ed A Anagnostopoulos, F Milia and A Simopoulos, abstracts p 272
[22] Vikhnin V S 1976 *Sov. Phys.–Solid State* **18** 853
[23] Hayes W, Owen I B and Walker P J 1977 *J. Phys. C: Solid State Phys.* **10** 1751
[24] Yamaga M and Hayes W 1982 *J. Phys. C: Solid State Phys.* **15** L1215
[25] Diegeler A, Haselhoff M and Siegert H 1998 *Solid State Commun.* **105** 269
[26] Abraham A and Bleaney B 1970 *Electron Paramagnetic Resonance of Transition Ions* (Oxford: Clarendon) p 456
[27] Abraham A and Bleaney B 1970 *Electron Paramagnetic Resonance of Transition Ions* (Oxford: Clarendon) p 801